New dinuclear zinc(II) complexes with Schiff bases obtained from o-phenylenediamine and their application as fluorescent materials in spin coating deposition

Magdalena Barwiolek[a,*], Dominika Jankowska[a], Mateusz Chorobinski[b], Anna Kaczmarek-Kędziera[a], Iwona Lakomska[a], Slawomir Wojtulewski[c] and Tadeusz M. Muziol[a]

[a] Faculty of Chemistry, Nicolaus Copernicus University in Torun, 87-100 Torun, Poland, e-mail: mbarwiolek@umk.pl (M.B.); dominikajankowska@doktorant.umk.pl (D.J); teoadk@chem.umk.pl (A.K.K.); iwolak@umk.pl (I.L.); tadeuszmuziol@wp.pl (T.M.M);
[b] Institute of Mathematics and Physics, UTP University of Science and Technology, 85-796 Bydgoszcz, Poland matcho005@utp.edu.pl (M.C);
[c] Faculty of Chemistry, University of Białystok, Ciolkowskiego 1K, Białystok, 15-245, Poland slawoj@uwb.edu.pl (S.W);
* mbarwiolek@umk.pl; Tel.: +48-56-611-4516;

Table of contents

Figure S17. Frontier molecular orbitals of **K2** for the most intensive transitions (PBE0/6-311++G(d,p)/PCM(acetonitrile)).

Table S6: Theoretical PBE0/6-311++G(d,p)/PCM(ACN) vertical excitation wavelengths λ [nm] for most intensive transitions together with the corresponding oscillator strengths f and the orbital contributions for investigated species.

Table S7. Relevant fluorescent data of studied complexes in solid state (λ_{em}, λ_{ex} [nm]).

Figure S18. Scanning images, magn. 20kx for: a) **K1**, magn.10kx b) **K2_2**, c) EDX **K2-1**

Figure S19. Ψ and Δ ellipsometric azimuths measured (dashed lines) and their model fits (red solid lines) for the complex **K1_1**. The value of χ^2 was 2.27.

Figure S20. a) The real part of the complex refractive index (n) for the examined films of Zn complexes (**K1**). b) The extinction coefficient (k) for the examined films of Zn complexes (**K1**).

Figure S21. a) The real part of the complex refractive index (n) for the examined films of Zn complexes (**K2**). b) The extinction coefficient (k) for the examined films of Zn complexes (**K2**).

Table S1. Crystal data and structure refinement for **K1** and **K2**.

Identification code	**K1**	**K2**
Empirical formula	$C_{31.40}$ $H_{30.80}$ N_4 O_6 Zn_2	C_{44} H_{52} N_4 O_8 Zn_2
Formula weight	690.94	895.63
Temperature [K]	100(2)	100(2)
Wavelength [Å]	0.7999	1.54184
Crystal system, space group	Triclinic, P-1	Monoclinic, $P2_1/n$
Unit cell dimensions [Å] and [º]	a = 8.4210(17) α= 84.53(3) b = 8.7490(17) β= 88.28(3) c = 10.713(2) γ = 65.61(3)	a = 8.44590(10) α= 90 b = 23.8241(3) β= 91.4230(10) c = 20.1246(3) γ = 90
Volume [$Å^3$]	715.5(3)	4048.14(9)
Z, Calculated density [Mg m^{-3}]	1, 1.603	4, 1.470
Absorption coefficient [mm^{-1}]	2.301	1.946
F(000)	355	1872
Crystal size [mm]	0.060 x 0.030 x 0.015	0.210 x 0.040 x 0.020
Theta range for data collection [º]	2.149 to 29.992	2.875 to 74.500

Limiting indices	-10<=h<=10 -10<=k<=10 -13<=l<=13	-10<=h<=10 -29<=k<=29 -25<=l<=24
Reflections collected/unique	8721 / 2601 [R(int) = 0.0591]	37479 / 8285 [R(int) = 0.0541]
Completeness to theta 29.732º [%]	89.6	100.0
Max. and min. transmission	0.966 and 0.874	0.961 and 0.750
Refinement method	Full-matrix least-squares on F^2	Full-matrix least-squares on F^2
Data/restraints/parameters	2601 / 11 / 217	8285 / 0 / 535
Goodness-of-fit on F^2	1.054	1.044
Final R Indices [I>2sigma(I)]	R_1 [a] = 0.0592, wR_2 [b] = 0.1518	R_1 [a] = 0.0495, wR_2 [b] = 0.1246
R indices (all data)	R_1 [a] = 0.0956, wR_2 [b] = 0.1805	R_1 [a] = 0.0608, wR_2 [b] = 0.1339
Largest diff. peak and hole [eÅ^{-3}]	0.947 and -0.527	1.423 and -0.764

[a] $R1 = \Sigma||F_0| - |F_c||/\Sigma|F_0|$

[b] $wR2 = [\Sigma w(F_0^2 - F_c^2)^2/\Sigma(w(F_0^2)^2)]^{1/2}$

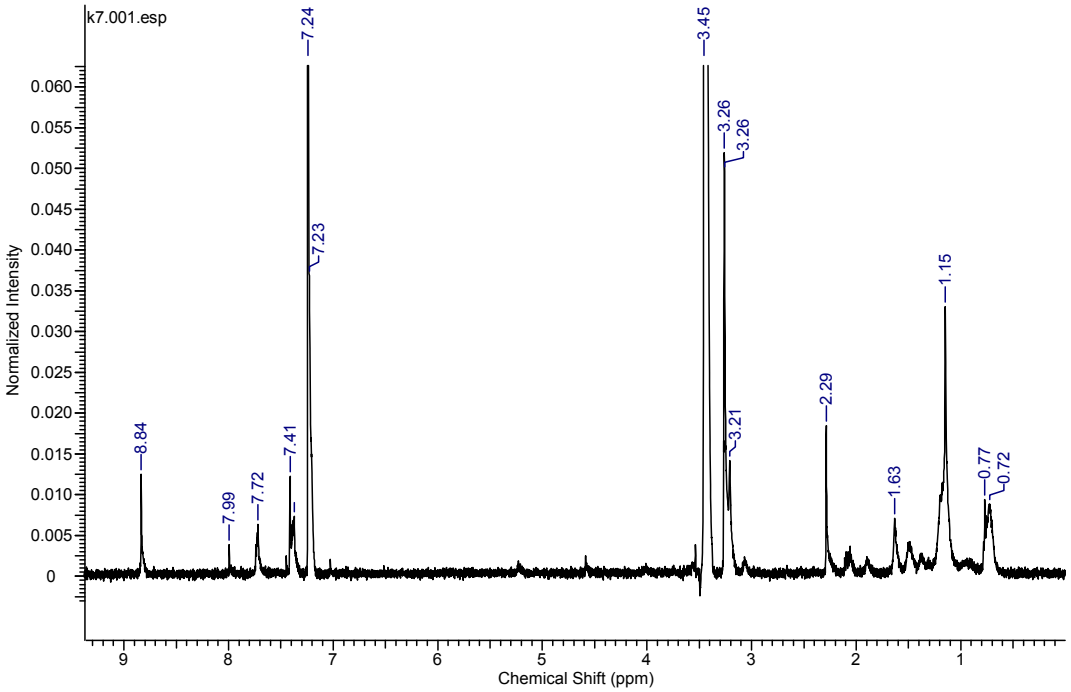

Figure S1. ^{1}H NMR spectrum of **K1** (500 MHZ, $CDCl_3$).

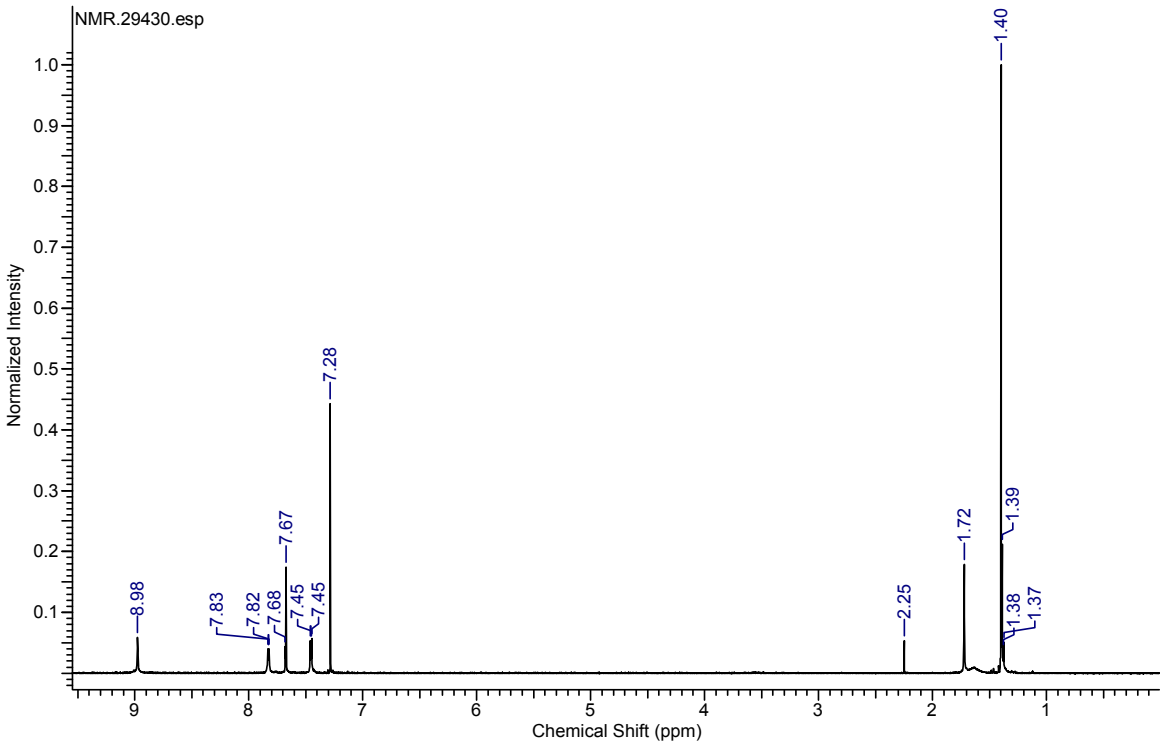

Figure S2. ^{1}H NMR spectrum of **K2** (700 MHZ, $CDCl_3$).

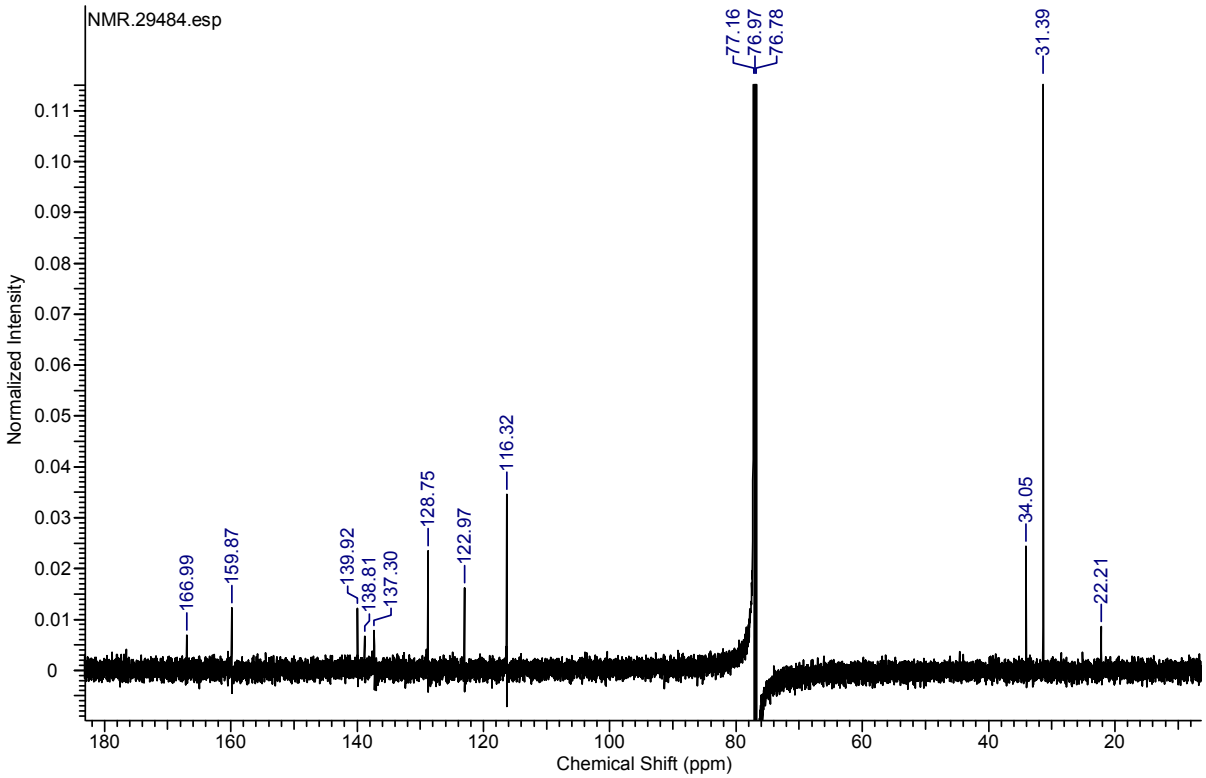

Figure S3. ^{13}C{1H} NMR spectrum of **K2** (700 MHZ, $CDCl_3$).

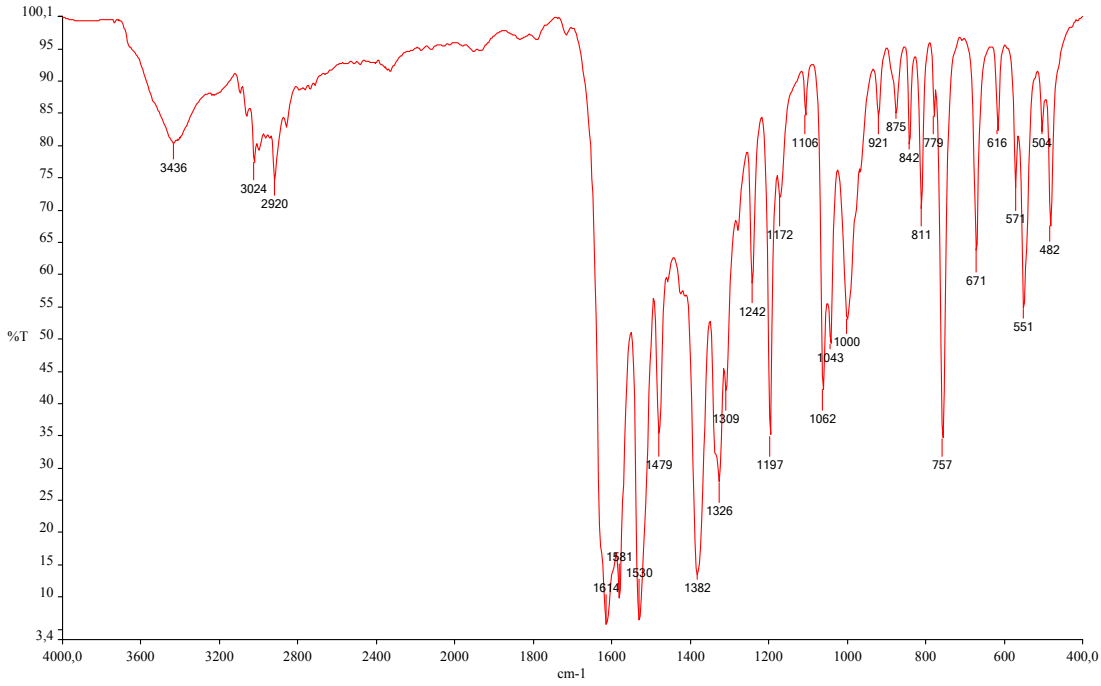

Figure S4. IR spectrum of **K1**, KBr.

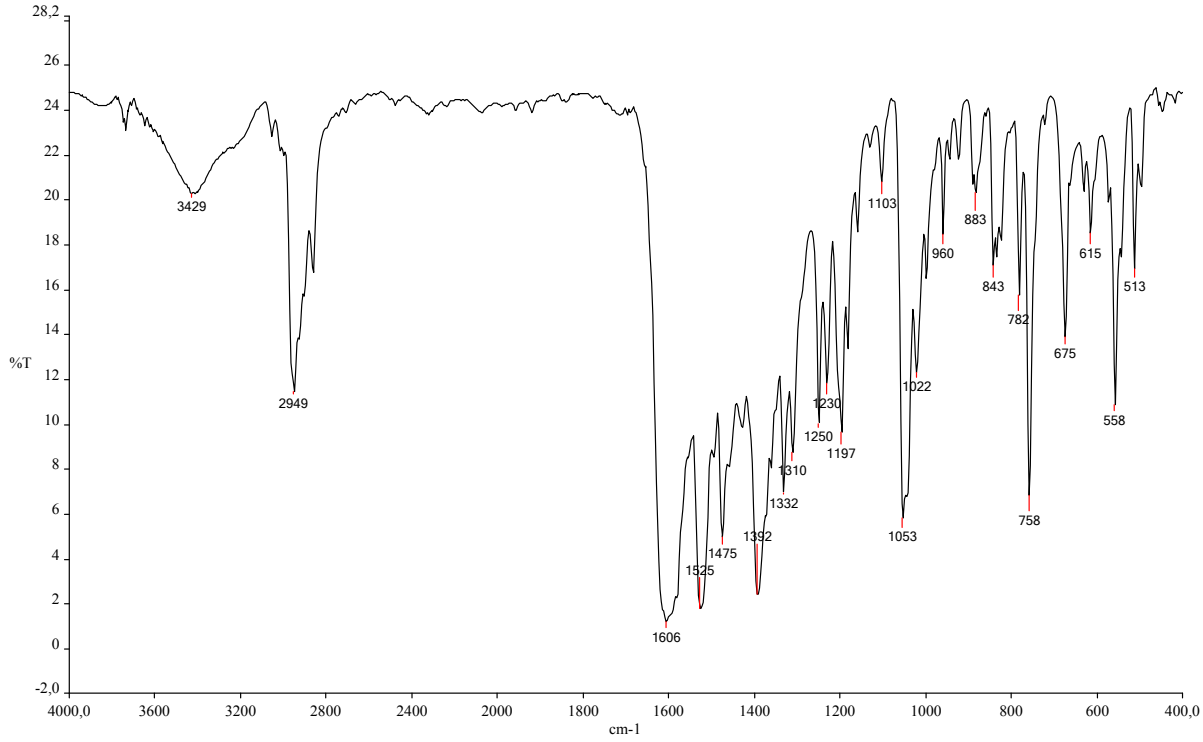

Figure S5. IR spectrum of **K2**, KBr.

Thermal analysis

For both complexes the thermal decomposition studies were performed in the presence of air.
The thermogram of **K1** (Figure S6) presents one DTG peaks with maximum at 424°C, the sample mass loss amount to 65 %. The mass change begins at temperature 30°C and ends at temperature 505 °C.
The thermogram of **K2** reveals one decomposition peak on the DTG curve with maximum at 424°C, the sample mass loss amount to 76 % (Figure S8). The mass change begins at temperature 36°C and ends at temperature 513°C. The residue of the sample after combustion was analyzed by calculation and XRD analysis (Figures S7, S9). The obtained data show that the final product of decomposition is ZnO.

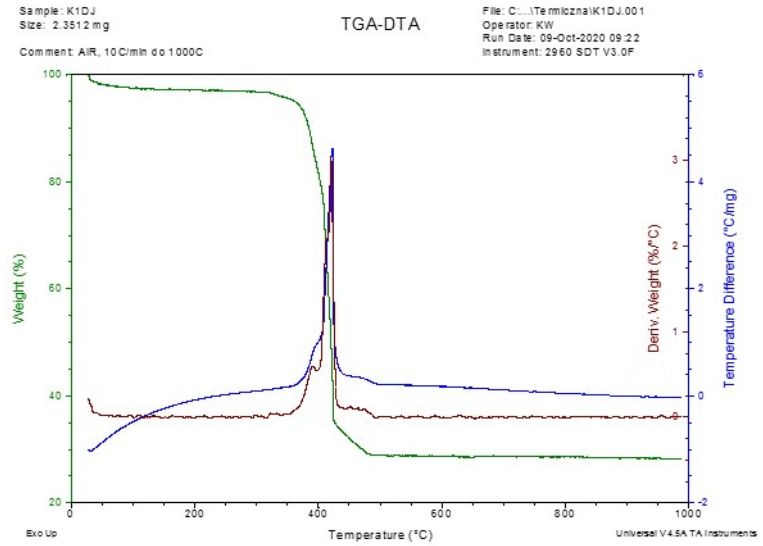

Figure S6. TG-DTA traces of **K1**.

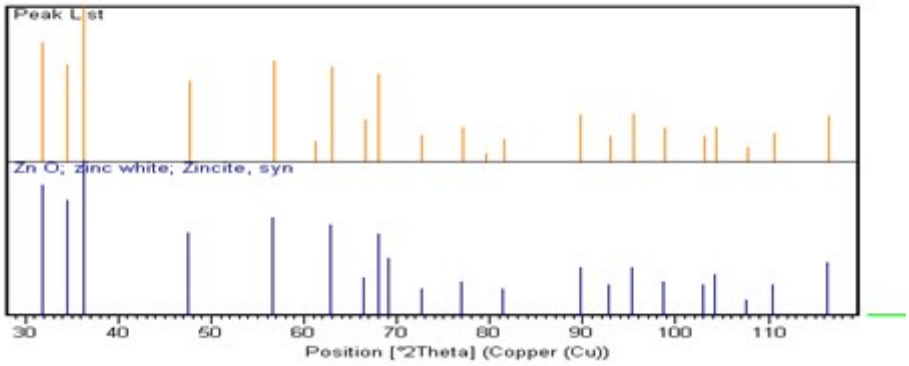

Figure S7. XRD analysis - Compliance of the sample **K1** composition with ZnO.

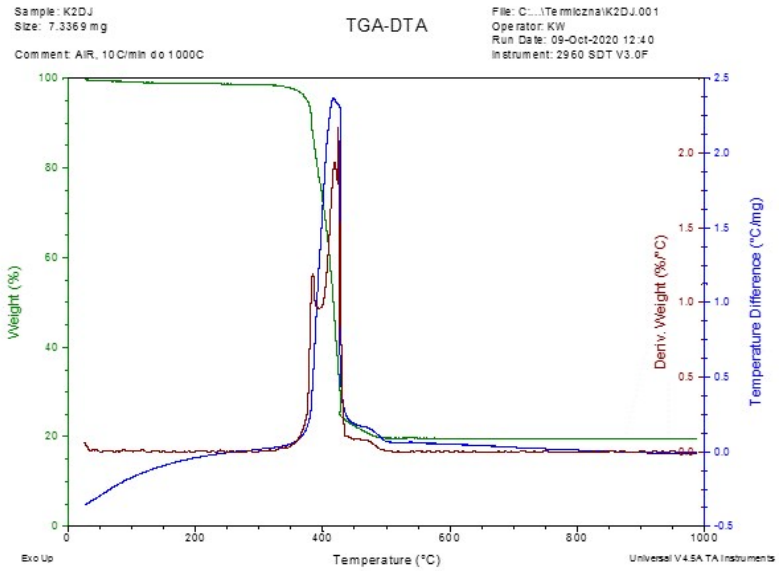

Figure S8. TG-DTA traces of **K2**.

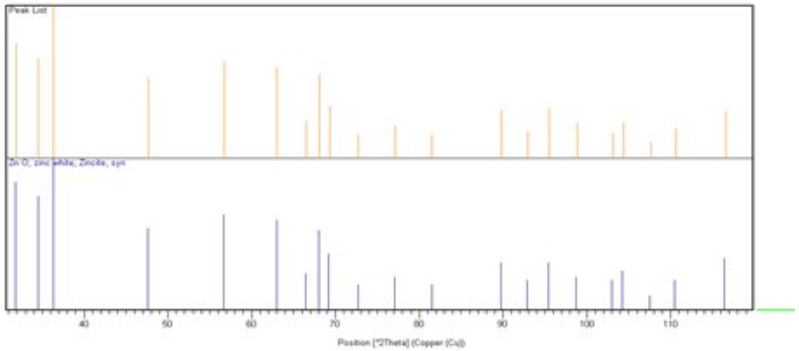

Figure S9. XRD analysis - Compliance of the sample **K2** composition with ZnO.

Table S2. Selected bond length [Å] and bond angles [°] for the complex **K1**.

K1			
Zn1-O14	2.014(5)	Zn1-N8	2.059(6)
Zn1-O14^{i}	2.029(5)	Zn1-N1	2.075(5)
Zn1-O17	2.022(9)	Zn1-Zn1^{i}	3.203(2)
N1-C1	1.283(9)	C8-N8	1.278(9)
N1-C2	1.406(8)	C7-N8	1.421(7)
C1-C13^{i}	1.458(9)	C8-C9	1.469(9)
	bond angles [°]		
O14-Zn1-O14^{i}	75.2(2)	N8-Zn1-N1	80.7(2)
O14-Zn1-N8	85.4(2)	O14-Zn1-O17	112.6(2)
O14^{i}-Zn1-N8	131.3(2)	O14^{i}-Zn1-O17	116.4(3)
O14-Zn1-N1	136.8(2)	N8-Zn1-O17	112.2(3)
O14^{i}-Zn1-N1	83.9(2)	N1-Zn1-O17	110.5(3)
Zn1-O14-Zn1^{i}	104.8(2)		
C1-N1-C2	124.6(5)	C8-N8-C7	123.8(6)
N1-C1-C13^{i}	124.9(6)	N8-C8-C9	126.2(6)

(**K1**) ^{i} -x,-y+1,-z+1,

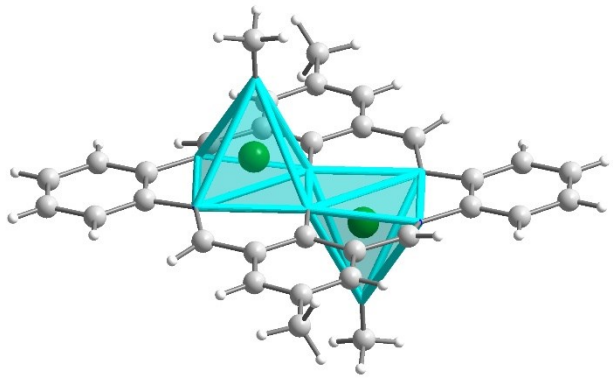

Figure S10. Structure of **K1** with square pyramids sharing the edge.

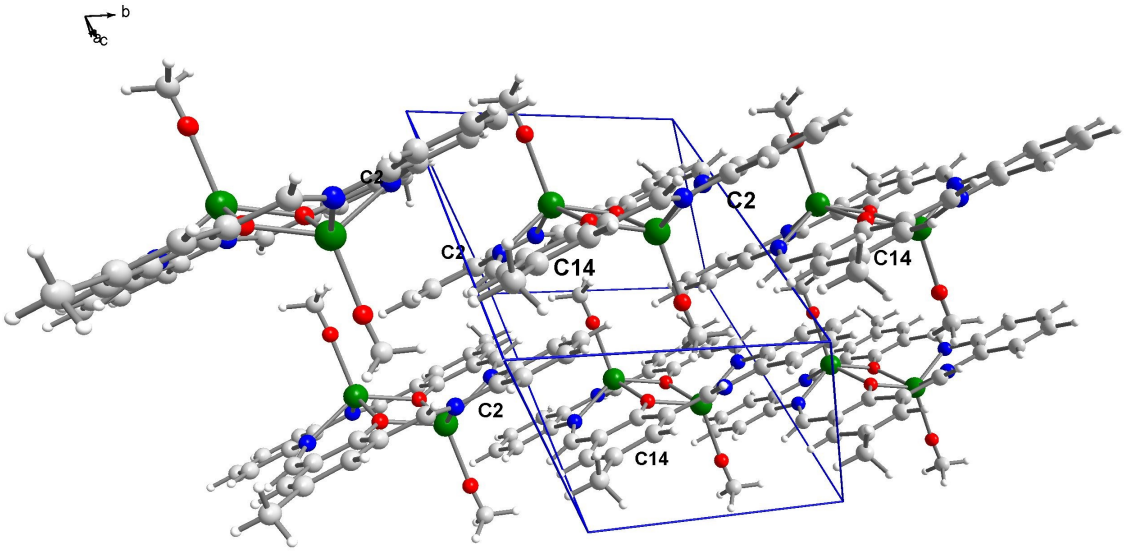

Figure S11. Stacking interactions between aromatic rings of complex molecules forming ab layer with labeled atoms mentioned the structure description (**K1**).

Table S3. Selected bond length [Å] and bond angles [°] for the complex **K2**

	bond length [Å]		
Zn(1)-O(41)	1.9482(18)	Zn(1)-N(8)	2.048(2)
Zn(1)-O(14)	1.9925(18)	Zn(1)-N(1)	2.069(2)
Zn(1)-O(34)	2.0384(17)		
C(1)-N(1)	1.290(3)	N(8)-C(8)	1.290(3)
N(1)-C(2)	1.422(3)	C(7)-N(8)	1.412(3)
C(1)-C(33)	1.467(3)	C(8)-C(9)	1.456(3)
Zn(2)-O(46)	1.9516(18)	Zn(2)-N(21)	2.072(2)
Zn(2)-O(14)	2.0368(17)	Zn(2)-N(28)	2.0506(19)
Zn(2)-O(34)	1.9944(18)	Zn(1)-Zn(2)	3.192

N(28)-C(28)	1.288(3)	N(8)-C(8)	1.290(3)
C(27)-N(28)	1.423(3)	C(7)-N(8)	1.412(3)
C(28)-C(29)	1.464(3)	C(8)-C(9)	1.456(3)
	bond angles [°]		
O(14)-Zn(1)-O(34)	75.28(7)	N(8)-Zn(1)-N(1)	81.17(8)
O(14)-Zn(1)-N(8)	86.80(7)	O(41)-Zn(1)-O(14)	117.55(8)
O(34)-Zn(1)-N(8)	133.81(8)	O(41)-Zn(1)-O(34)	109.72(8)
O(14)-Zn(1)-N(1)	136.03(8)	O(41)-Zn(1)-N(8)	116.30(8)
O(34)-Zn(1)-N(1)	83.15(8)	O(41)-Zn(1)-N(1)	105.63(8)
Zn(1)-O(14)-Zn(2)	104.76(8)	C(8)-N(8)-C(7)	124.5(2)
C(1)-N(1)-C(2)	124.2(2)	N(8)-C(8)-C(9)	125.5(2)
N(1)-C(1)-C(33)	124.0(2)		
O(34)-Zn(2)-O(14)	75.28(7)	N(28)-Zn(2)-N(21)	81.04(8)
O(14)-Zn(2)-N(21)	83.29(8)	O(46)-Zn(2)-O(14)	110.67(8)
O(34)-Zn(2)-N(21)	137.16(8)	O(46)-Zn(2)-O(34)	113.47(8)
O(14)-Zn(2)-N(28)	132.09(8)	O(46)-Zn(2)-N(28)	117.23(8)
O(34)-Zn(2)-N(28)	86.44(8)	O(46)-Zn(2)-N(21)	108.68(8)
Zn(2)-O(34)-Zn(1)	104.63(8)	C(21)-N(21)-C(22)	123.3(2)
C(28)-N(28)-C(27)	123.9(2)	N(21)-C(21)-C(13)	124.2(2)
N(28)-C(28)-C(29)	125.3(2)		

Table S4. Bond angles in the reported complexes **K1** and **K2**.

Torsion angle [°]	complex **K1**	Complex **K2***
$C13^{i}$ -C1-N1-C2	178.6(6)	-178.3(2), 177.1(2)
C1-N1-C2-C7	-163.4(6)	174.1(2), -166.2(2
N1-C2-C7-N8	-1.5(8)	-3.2(3), 0.9(3)
C2-C7-N8-C8	163.5(6)	-164.2(2), 167.1(2)
C7-N8-C8-C9	-176.5(6)	173.6(2), -173.7(2)
N8-C8-C9-C14	15.3(10)	-11.4(4), 9.9(4)
C8-C9-C14-C13	177.5(6)	-178.0(2), 175.8(2)
$C1^{i}$ -C13-C14-C9	179.6(6)	-174.8(2), 177.6(2)
C14 -C13 -$C1^{i}$ -$N1^{i}$	20.2(1.0)	-20.2(4), 17.6(4)

K1 ^{i} -x,-y+1,-z+1, in **K2*** contrary to **K1** the whole ring is found in the asymmetric unit and hence, the similar angles can differ. However, this column proves that they remained almost identical.

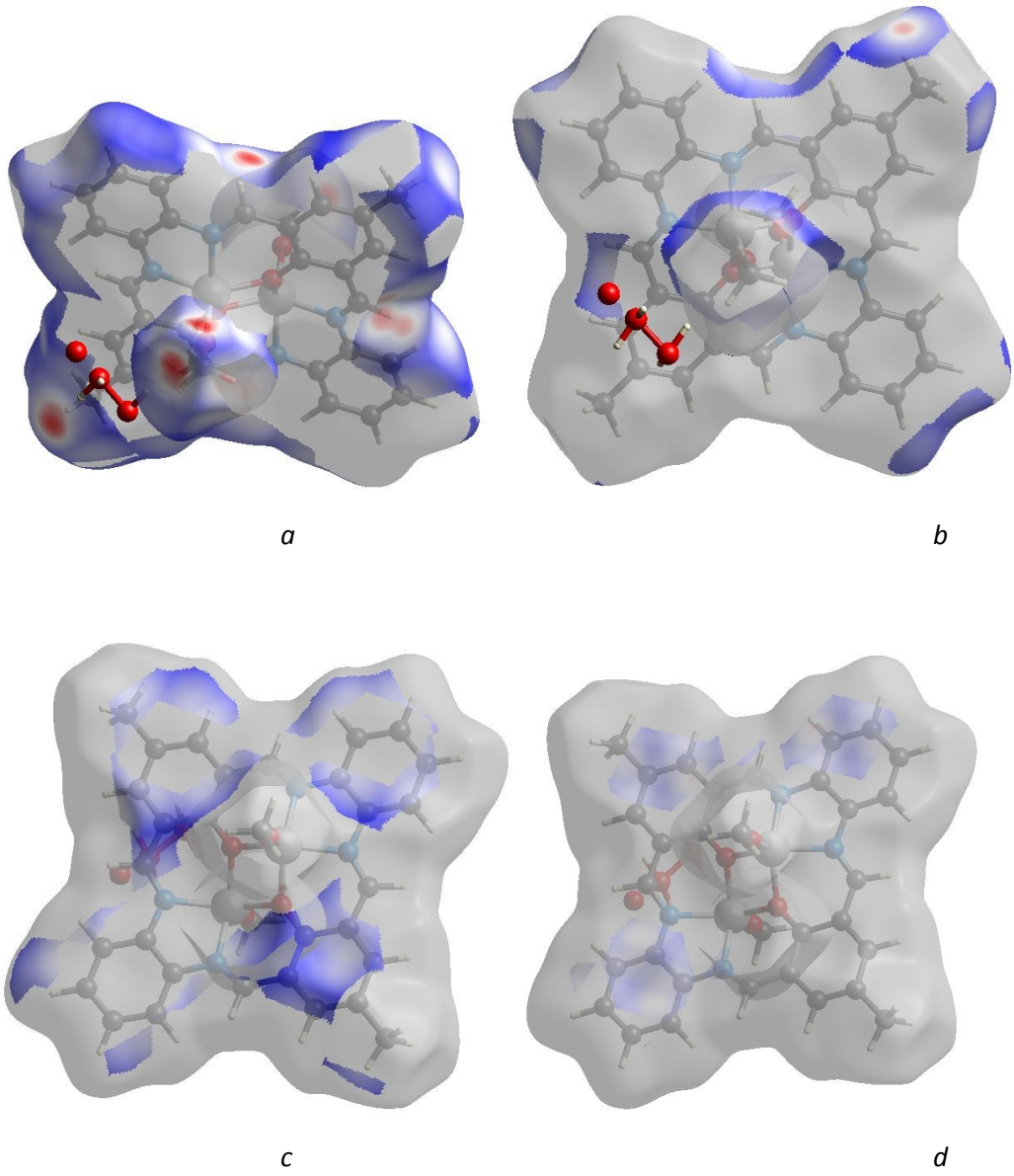

Figure S12. Selected (the most frequent and the closest) interactions projected onto Hirshfeld surfaces (a. H…H contacts 51.1%, b. H…O 15.7%, c. H…C 16.8, d. C…C 9.1%) for $[Zn_2(MeO)_{1.4}(OH)_{0.6}(L1)]\cdot 2H_2O$ **K1**.

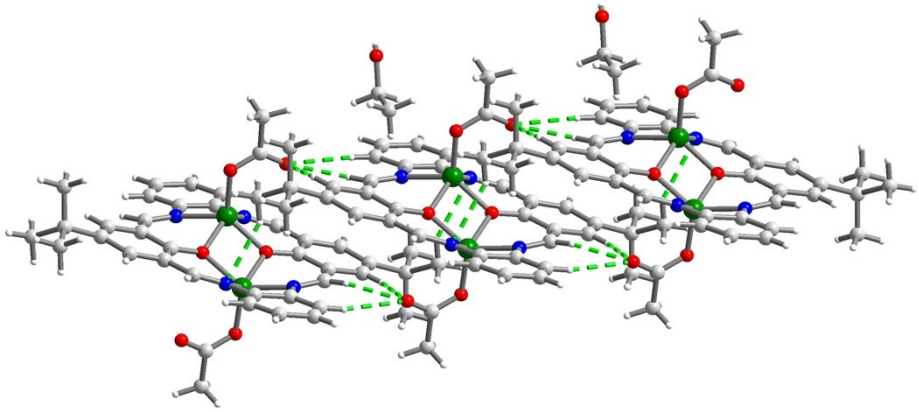

Figure S13. π-π interactions between complex molecules translated along a axis with marked in green C-H…O/N hydrogen bonds **K2**.

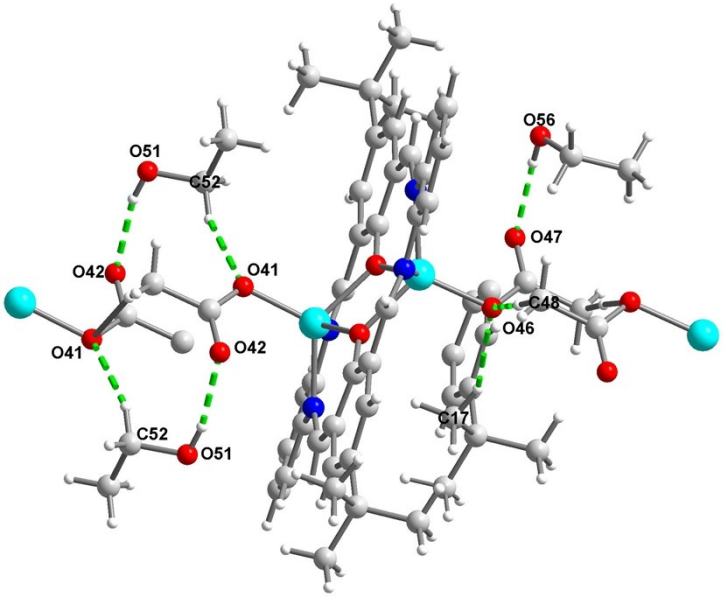

Figure S14. Hydrogen bond (marked in green) network formed by acetate anions and ethanol molecules in **K2**.

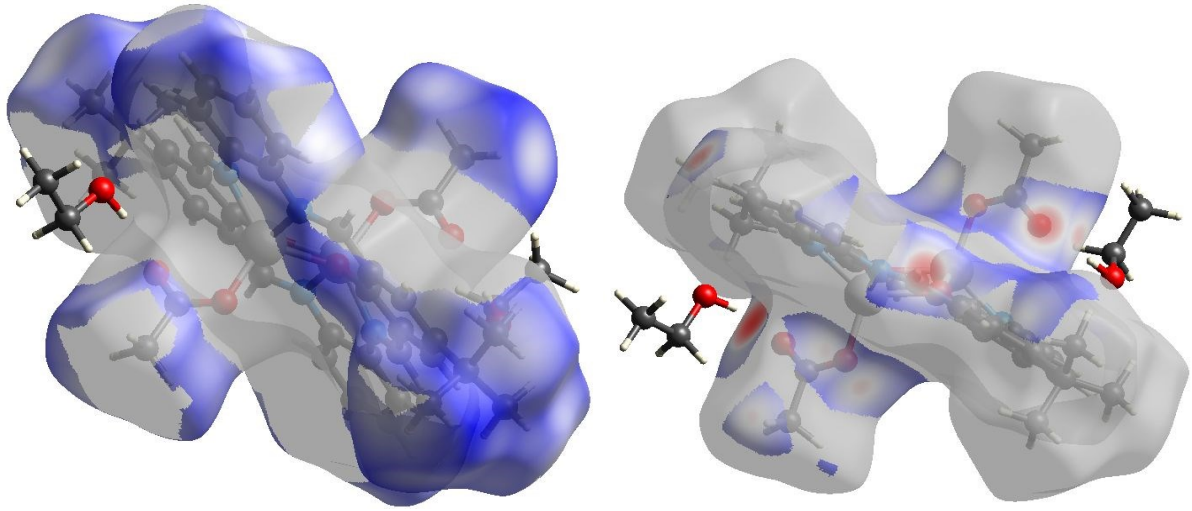

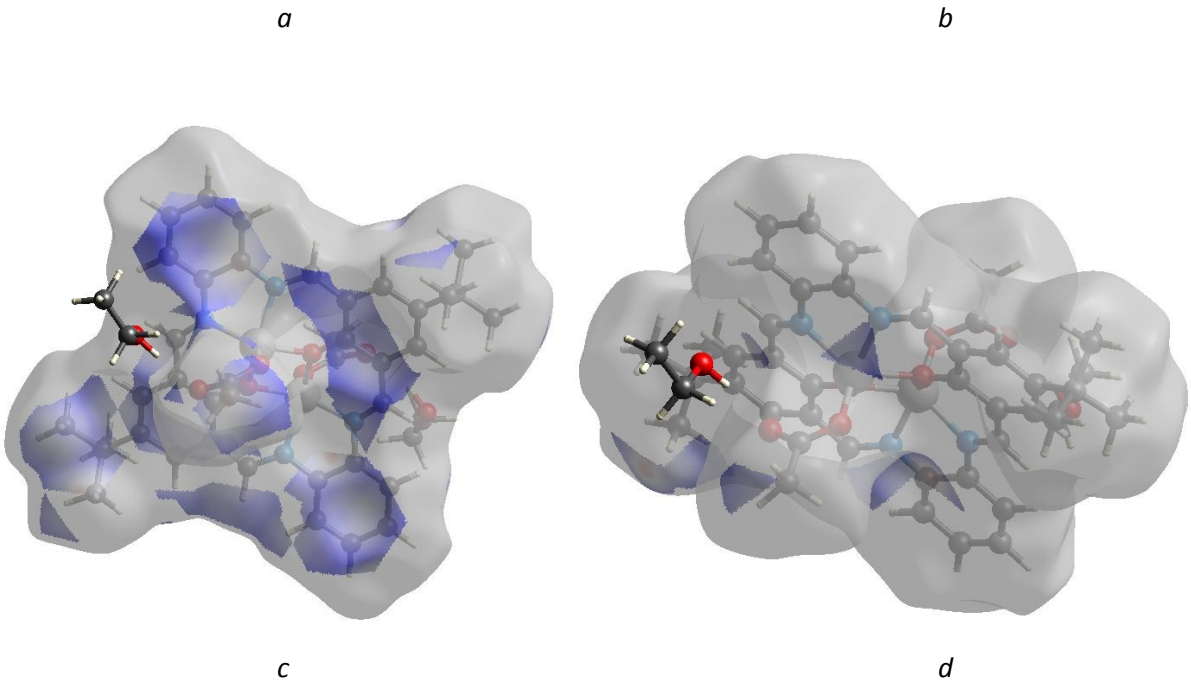

Figure S15. Selected (the most frequent and the closest) interactions projected onto Hirshfeld surfaces (a. H…H contacts 53.2%, b. H…O 15.7%, c. H…C 23.3%, d. H…N 4.7%) for $[Zn_2(CH_3COO)_2(L2)]\cdot 2EtOH$ **K2**.

Table S5. Relevant photophysical data of **K1** and **K2**, (λ_{em}, λ_{ex} nm, total fluorescence quantum yield **φ,** λ[nm] (ε [dm^3 mol^{-1} cm^{-1}]).

Compound	**Solvent**	**λ_{ex} [nm]**	**λ_{em} [nm]**	**φ**	**λ[nm] (ε [dm^3 mol^{-1} cm^{-1}])**	**Δ_v[a] (cm^{-1})**
K1	acetonitrile	420	556	0.07	324 (1430) 418 (1240) 588 (500)	5937
	chloroform	420	561	**0.3**	245 (13710) 295 (20210) 360 (10210) 425 (12870) 585 (1010)	5703
	methanol	420	550	0.21	328 (4270) 408 (3720) 584 (510)	6327
	benzene	420	573	0.05	336 (600) 586 (510)	

K2	acetonitrile	420	534	0.2	290 (17700) 414 (6320) 588 (70)	5427
	chloroform	420	550	0.1	290 (23510) 340 (18020) 420 (19450) 585 (100)	5628
	methanol	420	543	0.15	310 (11690) 414 (7710) 436 (6420) 586 (110)	5737
	benzene	420	544	**0.78**	302 (7070) 424 (5040) 588(450)	5202

[a] Stokes shifts

A. Hens, P. Mondal, K. K. Rajak, *Dalton Trans*., 2013, **42**, 14905

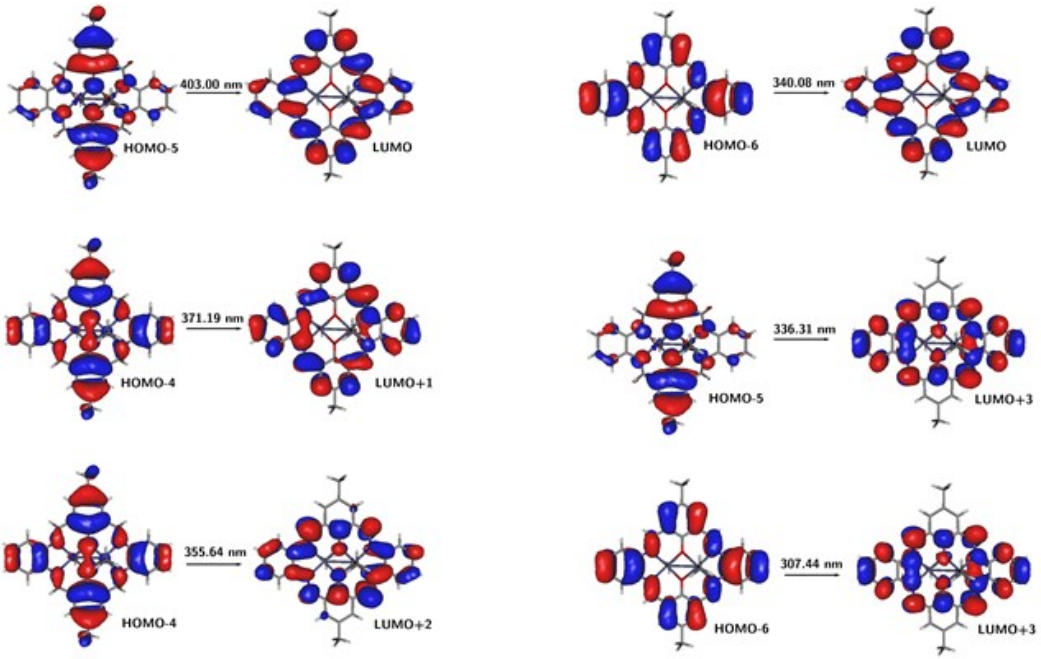

Figure S16. Frontier molecular orbitals of **K1** for the most intensive transitions (PBE0/6-311++G(d,p)/PCM(acetonitrile)).

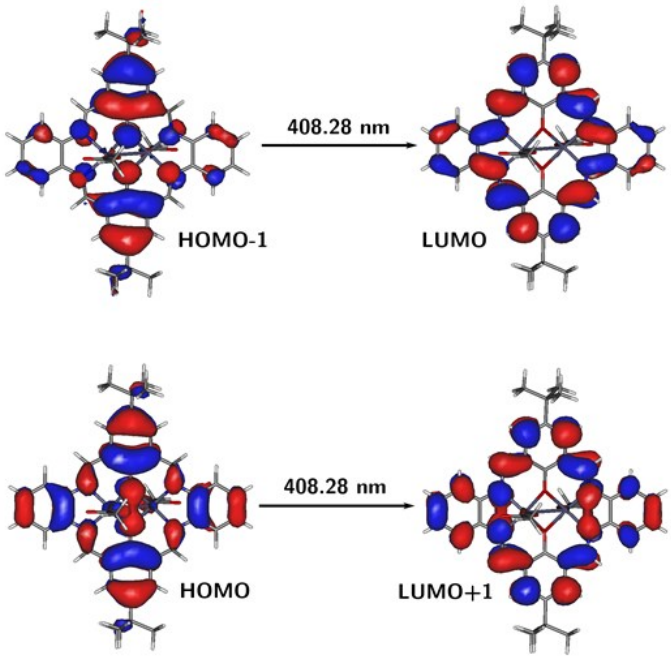

Figure S17. Frontier molecular orbitals of **K2** for the most intensive transitions (PBE0/6-311++G(d,p)/PCM(acetonitrile)).

Table S6. Theoretical PBE0/6-311++G(d,p)/PCM(ACN) vertical excitation wavelengths λ [nm] for most intensive transitions together with the corresponding oscillator strengths f and the orbital contributions for investigated species.

K1		
λ [nm]	f	Orbitals (contribution)
403.00	0.3805	HOMO-5->LUMO (91%)
371.19	0.2697	HOMO-4->LUMO+1 (92%)
355.64	0.1871	HOMO-4->LUMO+2 (75%)
340.08	0.1479	HOMO-6->LUMO (43%)
336.31	0.4682	HOMO-6->LUMO (42%) HOMO-5->LUMO+3 (41%)
307.44	0.4664	HOMO-6->LUMO+3 (86%)
K2		
408.27	0.4708	HOMO-1->LUMO (87%) HOMO->LUMO+1 (9%)
384.42	0.2113	HOMO->L+1 (89%) HOMO-1->LUMO (8%)

367.33	0.2356	HOMO->LUMO+2 (91%)
355.70	0.5862	HOMO-2->LUMO (85%)
315.25	0.2274	HOMO-3->LUMO+2 (29%), HOMO-2->LUMO+3 (33%)
314.82	0.2846	HOMO-2->LUMO+3 (55%)

Table S7. Relevant fluorescent and UV-Vis data of studied complexes in the solid state (λ_{em}, λ_{ex} [nm].

Compound	**λ_{ex} [nm]**	**λ_{em} [nm]**	**φ**	λ[nm]
K1	420	573	0.28	256 332 409 482
K2	420	556	0.58	267 392 473

Determination of the fluorescence quantum yield

The quantum yield was calculated by using following equation:

$$\Phi_x = \Phi_{ST} \text{ x } \left(\frac{I}{I_R} \text{ x } \frac{OD_R}{OD} \text{ x } \frac{\eta^2}{\eta_R^2}\right)$$

Φ_x - fluorescence quantum yield
OD –fluorescence intensity
I absorption
η refractive index of solvent
R- reference fluorophore of known quantum yield here chinine
$\Phi_{ST} = 0.54$

$$\frac{\eta^2}{\eta_R^2} = 1.021$$

[1] M.W. Allen, Thermo Scientific, technical note 52019.

[2] J. N. Demas, G. A. Crosby, The Measurement of Photoluminescence Quantum Yields.1 A Review2. *J. Phys. Chem*., 1971, *75(8)*, 991-1024.

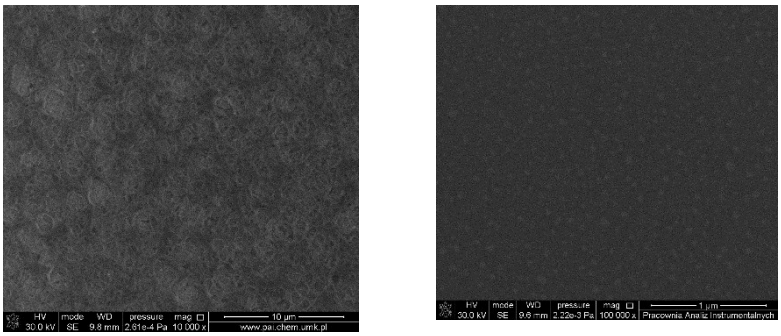

a) b)

c)

Figure S18. Scanning images, magn. 20kx for: a) **K1**, magn.10kx b) **K2_2**, c) EDX **K2-1**

Ellipsometric analysis of the thin films

The thickness and optical constants ($\grave{n}$ - the complex refractive index) of the prepared thin films were determined based on a four medium optical model of the sample (substrate – Si\native SiO_2 film\Zn complex film\ambient). The optical constants of the complex film were described as a sum of Gaussian oscillators [1]:

$$\hat{I}\mu = \hat{I}\mu_{\hat{a}^{\wedge}\check{z}} + \hat{a}_{j=1}^{m} Gauss(A_j, E_j, Br_j) \quad \text{, eq. 1}$$

where $\grave{\varepsilon}$ is the complex dielectric function ($\grave{\varepsilon} = \grave{n}^2$=(n+ik)^2, n – the real part of the complex dielectric function, k – the extinction coefficient). In Eq.1, ε_∞ is the high frequency dielectric constant, while A_j, E_j and Br_j are the amplitude, energy and broadening of the j-th absorption band, respectively. Mathematical formulas used to describe particular line shapes can be found in [1,2]. Optical constants of Si and SiO_2 were taken from the database of optical constants [2].

The model quantities were varied to minimize the reduced mean squared error (χ^2) [1,2]:

$$\chi^2 = \frac{1}{N-P}\sum_j \left[\frac{\Psi_j^{mod} - \Psi_j^{exp}}{\sigma_j^{\Psi}}\right]^2 + \left[\frac{\Delta_j^{mod} - \Delta_j^{exp}}{\sigma_j^{\Delta}}\right]^2, \quad \text{eq. 2}$$

In Eq.2, N and P are the total number of data points and the number of fitted model parameters, respectively. The Ψ_j^{exp} and Δ_j^{exp} are experimental ellipsometric azimuths, while the Ψ_j^{mod} and Δ_j^{mod} are values obtained during the fitting procedure. Quantities σ_j^{Ψ} and σ_j^{Δ} are standard deviations of Ψ and Δ data. The fit procedure was performed using the WASE32 software from J. A. Woollam Co., Inc.

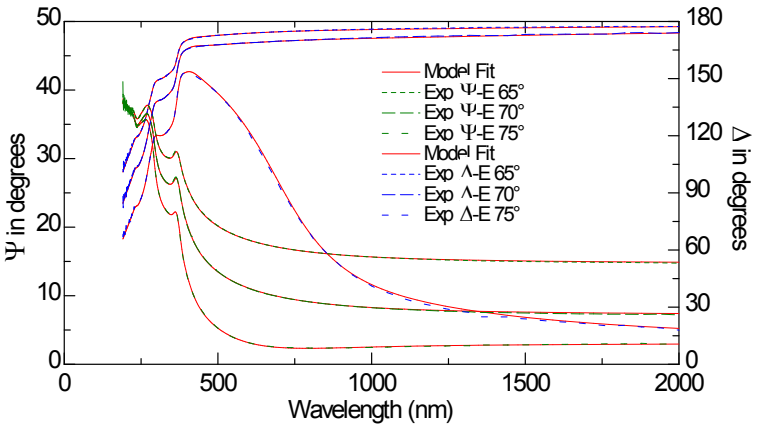

Figure S19. Ψ and Δ ellipsometric azimuths measured (dashed lines) and their model fits (red solid lines) for the complex **K1_1**. The value of χ^2 was 2.27.

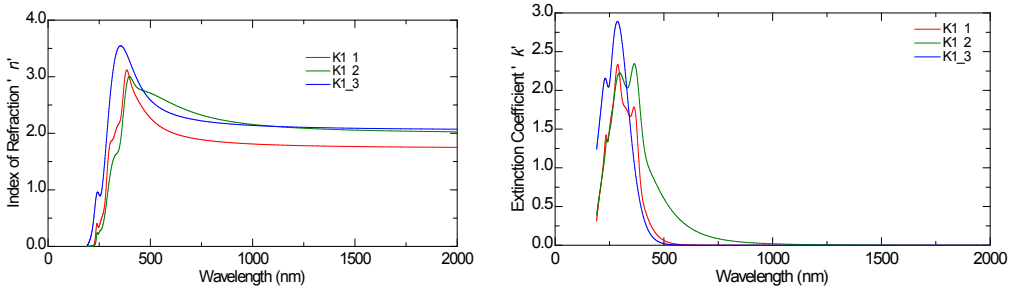

a) b)

Figure S20. a) The real part of the complex refractive index (n) for the examined films of Zn complexes (**K1**). b) The extinction coefficient (k) for the examined films of Zn complexes (**K1**).

Figure S19 shows the experimental Ψ and Δ azimuths for the Zn complex **K1_1**. The real part of the complex refractive index (n) and the extinction coefficient (k) for the examined films of Zn complexes are presented in Figures S20a and S20b. In the non-absorbing range, the value of the refractive index exhibits normal dispersion and is about 1.8 for the **K1_1** Zn complex and about 2.1 for the other Zn complex layers. The absorption threshold for **K1_1** and **K1_3** specimens is about 400-410 nm (see Figure S20b). For the **K1_2** Zn complex, the absorption threshold is shifted towards longer wavelengths; however, its value cannot be precisely determined (see the curve **K1_2** in Figure S20a). For short wavelengths (generally below 500 nm for **K1_1** and **K1_3** complexes and below about 700 nm for **K1_2** layer), the absorption bands are visible (see Figures S20a and S20b), and they were reproduced using the sum of Gaussian oscillators (see Eq.1). Absorption bands related to the π→π* transitions are described as a series of Gausssian oscillators with the maximum at 360 nm and 280 nm (for **K1_1** and **K1_3** samples) and at 280 nm (for **K1_2** Zn complex). The vibronic coupling between n→π* transitions is observed at 230 nm for all the **K1** Zn complexes.

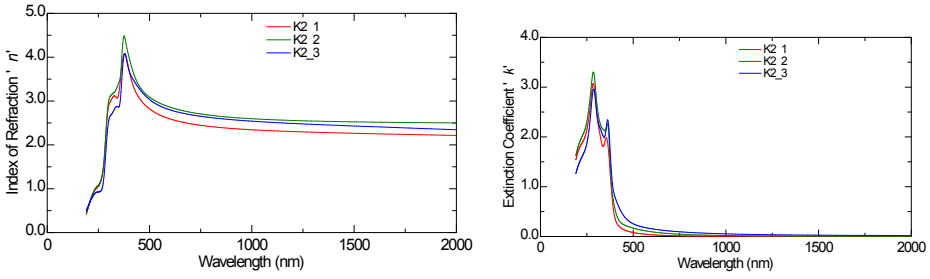

a) b)

Figure S21. **a)** The real part of the complex refractive index (n) for the examined films of Zn complexes (**K2**). **b)** The extinction coefficient (k) for the examined films of Zn complexes (**K2**).

The refractive index values for the **K2** series of samples established for long wavelengths (longer than 500 nm) are between 2.3 and 2.6 (see Figure 21a) and are larger than those obtained for the **K1_1**, **K1_2** and **K1_3** samples. The threshold wavelength is about 400 nm for all the films prepared (see Figure 21b) however, non-zero absorption can be observed for longer wavelengths. The peaks observed in the k spectra are associated with $\pi \rightarrow \pi^*$ (280 nm) and $n \rightarrow \pi^*$ (360 nm) transitions in the aromatic ring.

Figure S14 shows the experimental Ψ and Δ azimuths for the Zn complex **K1_1**.

The legend of the obtained samples:
K1_1 $[Zn_2(MeO)_{1.4}(OH)_{0.6}(L1)]\cdot 2H_2O$ **K1**, PS/Si: PS 2000 rpm, 5s x2, $[Zn_2(MeO)_{1.4}(OH)_{0.6}(L1)]\cdot 2H_2O$ **K1** 2000 rpm 5s x3
K1_2 $[Zn_2(MeO)_{1.4}(OH)_{0.6}(L1)]\cdot 2H_2O$ **K1**, PS/Si: PS 2000 rpm, 5s x1, $[Zn_2(MeO)_{1.4}(OH)_{0.6}(L1)]\cdot 2H_2O$ **K1**1500 rpm 5s x2

K1_3 $[Zn_2(MeO)_{1.4}(OH)_{0.6}(L1)]\cdot 2H_2O$ $2H_2O$ **K1**, PS/Si: $[Zn_2(MeO)_{1.4}(OH)_{0.6}(L1)]\cdot 2H_2O$ **K1** 1500 rpm 5s x4

K2_1 $[Zn_2(CH_3COO)_2(L2')]\cdot 2EtOH$ **K2**, PS/Si: PS+$[Zn_2(CH_3COO)_2(L2')]\cdot 2EtOH$ **K2** 3000 rpm 5s x5, $[Zn_2(CH_3COO)_2(L2')]\cdot 2EtOH$ **K2** 3000 rpm 5s x8, $[Zn_2(CH_3COO)_2(L2')]\cdot 2EtOH$ **K2** 3000 rpm 5s x8, suspension of $[Zn_2(CH_3COO)_2(L2')]\cdot 2EtOH$ **K2** 1500 rpm 5s x10
K2_2 $[Zn_2(CH_3COO)_2(L2')]\cdot 2EtOH$ **K2**, PS/Si: PS+$[Zn_2(CH_3COO)_2(L2')]\cdot 2EtOH$ **K2** 3000 rpm 10s x6, suspension of $[Zn_2(CH_3COO)_2(L2')]\cdot 2EtOH$ 3000 rpm 10s x6,

K2_3 $[Zn_2(CH_3COO)_2(L2')]\cdot 2EtOH$ **K2**, PS/Si: PS+$[Zn_2(CH_3COO)_2(L2')]\cdot 2EtOH$ **K2** 2500 rpm 5s x7, $[Zn_2(CH_3COO)_2(L2')]\cdot 2EtOH$ **K2** 2500 rpm 5s x8, suspension of $[Zn_2(CH_3COO)_2(L2')]\cdot 2EtOH$ **K2** 1500 rpm 5s x10.

1. H. Fujiwara, Spectroscopic Ellipsometry. Principles and Applications, John Wiley & Sons Ltd, Chichester, UK, **2009**.
2. J.A. Woollam Co., Inc, Guide to Using WVASE32®, Wextech Systems Inc., 310 Madison Avenue, Suite 905, New York, NY 10017, **2010**.